



Supplement of

Performance evaluation of portable dual-spot micro-aethalometers for source identification of black carbon aerosols: application to wildfire smoke and traffic emissions in the Pacific Northwest

Mrinmoy Chakraborty et al.

Correspondence to: Naomi Zimmerman (nzimmerman@mech.ubc.ca)

The copyright of individual parts of the supplement might differ from the article licence.

Section A: Abbreviations and notations used in this study

| | |
|--|--|
| eBC | Equivalent black carbon concentration. Aethalometer reported black carbon. |
| MAC | Mass Absorption Cross section |
| BC | Black Carbon |
| ATN₁, ATN₂ | Light attenuation measured in aethalometer from the photometer readings at filter spot 1 and filter spot 2 |
| PM_{2.5} | Particles with size up to 2.5 μm |
| I₀, I₁, I₂ | Light intensity measured by photometer from reference spot, aerosol loaded spot 1 and aerosol loaded spot 2 respectively |
| b_{abs,λ} | Light Absorption Coefficient at wavelength λ nm |
| b_{abs,NC} | Non-corrected b _{abs} derived from MA300 raw photometer data |
| b_{abs,D} | Drinovec-corrected b _{abs} derived from MA300 raw photometer data |
| α | Ångström exponent |
| α_{ff} | Constrained value of Ångström exponent for fossil fuel-based aerosol |
| α_{bb} | Constrained value of Ångström exponent for biomass burning based aerosol |
| C | Scattering correction factor |
| ξ | Lateral leakage factor on the aethalometer filter |
| k | Loading correction factor |
| A | Area of loaded filter spot on aethalometer |
| F₁, F₂ | Aerosol laden air flow rate on filter spot 1 and filter spot 2 |
| MA300 eBC | eBC reported by MA300 units which uses onboard correction scheme |
| MA300 b_{abs} | b _{abs} derived from MA300 reported data which uses onboard correction scheme |
| eBC_{bb} | Apportioned eBC component from biomass burning based sources |
| eBC_{ff} | Apportioned eBC component from fossil fuel-based sources |
| BB(%) | Percentage of eBC _{bb} component from total eBC. |

Section B: MA300 onboard correction method

The corrected eBC concentration is calculated by equation S1.

$$eBC_c = \frac{eBC_1}{(1 - k \times ATN_1)} \dots (S1)$$

Where, eBC_c is the compensated eBC concentration after the correction, k is the loading correction factor, ATN₁ refers the ATN values from channel 1 and eBC₁ refers to the non-corrected measurement

corresponding to spot 1, given by MA300s. As identified by Drinovec (Drinovec et al., 2015), the above compensation equation (S1) is similar but not the same to Virkkula's equation (Virkkula et al., 2007).

Moreover, Virkkula's (Virkkula et al., 2007) loading correction factor is calculated based on the data continuity from each filter spot. MA300 uses non-corrected eBC and ATN measurements from both the spots at each time stamp to estimate the compensation parameter and is given by equation S2.

$$k = \frac{BC_2 - BC_1}{(BC_2 \times ATN_1) - (BC_1 \times ATN_2)} \dots (S2)$$

It is important to note that MA300's data include both raw photometer readings and the compensated eBC concentrations for each wavelength channel, which provides opportunity to adapt AE33's algorithm and check for opportunities in improvement.

Section C: Data cleaning in MA300's raw data

Raw photometer sensor measurements from MA300s were subjected to drifts across the measurement period. These drifts can be attributed voltage fluctuation in the sensor readings in MA300. This is probably due to low quality (or low cost) photometer used in MA300 as compared to AE33. These drift in sensor readings; we are considering as outliers in the data collection. Based on inter quartile range (IQR) criteria, we have removed the drift points and results are shown in figure below (before and after removing outliers). The IQR criterion means that all observations above $q0.75 + 1.5IQR$ or below $q0.25 - 1.5IQR$ (where $q0.25$ and $q0.75$ correspond to first and third quartile respectively, and IQR is the difference between the third and first quartile) are considered as potential outliers by R programming software.

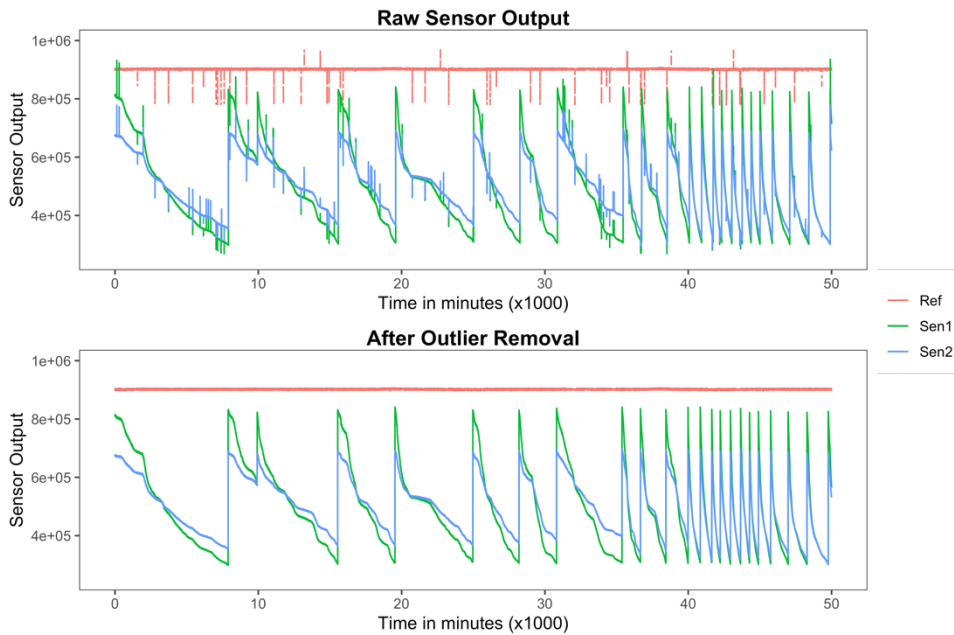


Figure S1: Sample sensor readings (left panel with drifts, right panel after noise removal) from MA300 in Reference spot (Ref), Spot 1 (Sen1) and Spot 2 (Sen2).

Section D: Aethalometer model for eBC source apportionment

Aethalometer model have been developed by utilizing the power law relationship of aerosol light absorption (Main text, equation 6). The two components model assumes light absorption is contributed by the two potential sources (eg. Biomass burning and fossil fuel emission), which has been widely considered in estimating BC emission (Sandradewi et al., 2008; Rajesh and Ramachandran, 2017; Dumka et al., 2018; Healy et al., 2019). This model apportions the total spectral b_{abs} into $b_{abs,ff}$ (light absorption from fossil fuel emission) and $b_{abs,bb}$ (light absorption from biomass burning emission) and subsequently estimated the eBC_{bb} and eBC_{ff} concentrations. Equations S3 – S9, have been derived and used to estimating the source contributions at each timestamp of data collected. In this work, we utilized α values from two particular previous work: (1) performed at the similar site (Healy et al., 2019) and (2) recommend values from 14C based analysis (Zotter et al., 2017).

$$b_{abs}(\lambda) = b_{abs,ff}(\lambda) + b_{abs,bb}(\lambda) \quad \dots \text{ (S3)}$$

$$\frac{b_{abs,ff}(\lambda_1)}{b_{abs,ff}(\lambda_2)} = \left(\frac{\lambda_1}{\lambda_2}\right)^{-\alpha_{ff}} \quad \dots \text{ (S4)}$$

$$\frac{b_{abs,bb}(\lambda_1)}{b_{abs,bb}(\lambda_2)} = \left(\frac{\lambda_1}{\lambda_2}\right)^{-\alpha_{bb}} \quad \dots \text{ (S5)}$$

$$b_{abs,bb} = \frac{b_{abs}(\lambda_1) - b_{abs}(\lambda_2) \times \left(\frac{\lambda_1}{\lambda_2}\right)^{-\alpha_{ff}}}{\left(\frac{\lambda_1}{\lambda_2}\right)^{-\alpha_{bb}} - \left(\frac{\lambda_1}{\lambda_2}\right)^{-\alpha_{ff}}} \quad \dots \text{ (S6)}$$

$$b_{abs,ff} = \frac{b_{abs}(\lambda_1) - b_{abs}(\lambda_2) \times \left(\frac{\lambda_1}{\lambda_2}\right)^{-\alpha_{bb}}}{\left(\frac{\lambda_1}{\lambda_2}\right)^{-\alpha_{ff}} - \left(\frac{\lambda_1}{\lambda_2}\right)^{-\alpha_{bb}}} \quad \dots \text{ (S7)}$$

$$eBC_{ff} = \frac{b_{abs,ff}(\lambda)}{MAC_{880}} \quad \dots \text{ (S8)}$$

$$eBC_{bb} = \frac{b_{abs,bb}(\lambda)}{MAC_{880}} \quad \dots \text{ (S9)}$$

Section E: Statistical comparison matrices

Systematic, quantitative performance analysis of MA300 derived quantities were done by utilizing different statistics metrics. To assess the consistency of MA300 reported data, we compared the results of MA300 units with the reference AE33 measurements and used single value performance matrices. We compare AE33's eBC concentration, multi-wavelength $b_{abs,\lambda}$ with MA300 instrument reported data. In addition to comparing instrument reported data, we normalized individual groups of data for each device separately and reported the relative performance with respect to AE33. Data normalization was done using min-max criteria (Géron, 2022). The parameters that were used in this study include: slope, coefficient of determination (R^2), mean absolute error (MAE), root mean squared error (RMSE), root mean squared error of normalized data (NRMSE). These parameters were selected based on previous studies which are focused on instrumental performance (Zimmerman, 2022; Malings et al., 2019), comparison studies (Alas et al., 2020; Rajesh and Ramachandran, 2018), or model evaluation (Zambrano-Bigiarini, 2020; Yao et al., 2013). The equations which are used to calculate the parameters are given as follows:

$$MAE_{ij} = \frac{1}{n_j} \sum |P_{AE33,j} - P_{MA300,i,j}|$$
$$RMSE_{ij} = \sqrt{\frac{\sum_1^n (P_{AE33,j} - P_{MA300,i,j})^2}{n_j}}$$
$$NRMSE_{ij} = \sqrt{\frac{\sum_1^n (N_{AE33,j} - N_{MA300,i,j})^2}{n_j}}$$
$$N_{normalized} = \frac{N - N_{min}}{N_{max} - N_{min}}$$

* P_{AE33} and P_{MA300} represents absolute measurements of parameters (eg. eBC) from AE33 and MA300 respectively for i^{th} MA300 device at j^{th} period (Regular or Wildfire). N_{AE33} and N_{MA300} represents the normalized values for individual instruments. For any parameter N , normalized quantity ($N_{normalized}$) was derived by the respective range, i.e. the difference in the maximum (N_{max}) and minimum (N_{min}) values.

Table S1: Wavelength of light absorption measurement and corresponding Mass Absorption Cross section (MAC) for AE33 and MA300 considered in this study

| <i>Channel</i> | <i>AE33</i> | | <i>MA300</i> | |
|----------------|------------------------|------------------------------|------------------------|------------------------------|
| | <i>Wavelength (nm)</i> | <i>MAC (m²/g)</i> | <i>Wavelength (nm)</i> | <i>MAC (m²/g)</i> |
| 1 | 370 | 18.47 | 375 | 24.069 |
| 2 | 470 | 14.54 | 470 | 19.07 |
| 3 | 520 | 13.14 | 528 | 17.028 |
| 4 | 590 | 11.58 | 625 | 14.091 |
| 5 | 660 | 10.35 | 880 | 10.12 |
| 6 | 880 | 7.77 | -- | -- |
| 7 | 950 | 7.19 | -- | -- |

Table S2: MA300 and AE33: Instrumental comparison and operational details

| | AE33 | MA300 |
|--------------------------------------|-----------------------------------|---------------------------------|
| Weight | 20 kg (approx.) | 0.715 kg |
| Power Requirement | AC (25 W typical) | AC + Battery Operated (46.08Wh) |
| Instrument Type | Dual Spot Aethalometer | Dual-Spot Micro-Aethalometer |
| Filter type | Teflon | PTFE |
| Sampling Spot Area | 0.785 cm ² | 0.07 cm ² |
| Wavelengths of Light Absorption (nm) | 370, 470, 520, 590, 660, 880, 950 | 375, 470, 528, 625, 880 |
| Filter Loading Correction | Using Drinovec 2015 | Using Virkkula 2007 |
| Scattering Correction | Using Drinovec 2015 | Not Considered |
| Operational Details | | |
| Flow Rate | 5000 ml per minute | 150 ml per minute |
| ATN range | 0-120 | 0-100 |
| Data Collection | 1 min | 1 min |

Table S3 (a). Table of statistical parameters for the MA300 units vs AE33 : eBC

| Period | eBC | MAE ($\mu\text{g}/\text{m}^3$) | RMSE ($\mu\text{g}/\text{m}^3$) | NRMSE (%) |
|--------|--------|-------------------------------------|--------------------------------------|--------------|
| Reg | MA300A | 0.41 | 0.61 | 8.41 |
| | MA300B | 0.44 | 0.66 | 8.96 |
| | MA300C | 0.44 | 0.66 | 8.23 |
| WF | MA300A | 0.87 | 1.14 | 11.10 |
| | MA300B | 1.18 | 1.55 | 15.43 |
| | MA300C | 0.86 | 1.16 | 10.90 |

Table S3 (b). Table of statistical parameters for the MA300 units vs AE33 : b_{abs}

| Period | b_{abs} | Channel | MAE (Mm^{-1}) | RMSE (Mm^{-1}) | NRMSE (%) |
|--------|------------------|---------|-----------------------------|------------------------------|--------------|
| Reg | MA300A | UV | 9.24 | 13.60 | 7.88 |
| | | Blue | 7.47 | 10.97 | 8.43 |
| | | Green | 6.51 | 9.54 | 8.36 |
| | | Red | 5.57 | 8.17 | 8.33 |
| | | IR | 3.87 | 5.74 | 8.41 |
| | MA300B | UV | 8.83 | 13.05 | 8.36 |
| | | Blue | 6.87 | 10.05 | 8.74 |
| | | Green | 5.91 | 8.64 | 8.70 |
| | | Red | 4.72 | 6.88 | 8.74 |
| | | IR | 3.35 | 4.90 | 8.96 |
| | MA300C | UV | 13.08 | 19.30 | 7.99 |
| | | Blue | 10.70 | 15.91 | 8.67 |
| | | Green | 9.14 | 13.57 | 8.49 |
| | | Red | 7.91 | 11.68 | 8.47 |
| | | IR | 5.43 | 8.01 | 8.23 |
| WF | MA300A | UV | 35.67 | 46.16 | 14.43 |
| | | Blue | 19.51 | 26.12 | 11.88 |
| | | Green | 16.06 | 21.01 | 11.81 |
| | | Red | 14.71 | 18.51 | 11.17 |
| | | IR | 9.58 | 12.10 | 11.10 |
| | MA300B | UV | 39.96 | 51.21 | 15.49 |
| | | Blue | 18.33 | 23.90 | 12.15 |
| | | Green | 14.23 | 18.75 | 12.61 |
| | | Red | 10.13 | 13.63 | 14.10 |
| | | IR | 6.99 | 9.38 | 15.43 |
| | MA300C | UV | 37.01 | 48.51 | 18.37 |
| | | Blue | 23.45 | 31.08 | 12.08 |
| | | Green | 19.42 | 25.54 | 11.71 |
| | | Red | 18.31 | 23.02 | 12.03 |
| | | IR | 13.24 | 16.20 | 10.90 |

Table S3 (C). Table of statistical parameters for the MA300 units vs AE33 : b_{absD}

| Period | b_{abs} | Channel | MAE (Mm^{-1}) | RMSE (Mm^{-1}) | NRMSE (%) |
|---------------|-----------------------------|----------------|---------------------------------------|--|----------------------|
| Reg | MA300A | UV | 13.42 | 20.38 | 8.81 |
| | | Blue | 10.45 | 15.63 | 9.27 |
| | | Green | 8.95 | 13.31 | 9.08 |
| | | Red | 7.65 | 11.28 | 8.93 |
| | | IR | 5.15 | 7.67 | 8.56 |
| | MA300B | UV | 10.78 | 15.91 | 9.90 |
| | | Blue | 8.24 | 12.04 | 10.24 |
| | | Green | 7.11 | 10.42 | 10.12 |
| | | Red | 5.93 | 8.69 | 9.79 |
| | | IR | 4.23 | 6.16 | 9.13 |
| | MA300C | UV | 16.79 | 24.92 | 8.67 |
| | | Blue | 13.32 | 19.62 | 9.21 |
| | | Green | 11.34 | 16.64 | 8.93 |
| | | Red | 9.87 | 14.47 | 8.93 |
| | | IR | 6.82 | 9.93 | 8.66 |
| WF | MA300A | UV | 48.84 | 62.14 | 22.44 |
| | | Blue | 26.62 | 34.80 | 16.00 |
| | | Green | 24.59 | 31.76 | 12.32 |
| | | Red | 21.99 | 27.62 | 11.59 |
| | | IR | 13.14 | 16.20 | 10.62 |
| | MA300B | UV | 46.69 | 62.10 | 24.95 |
| | | Blue | 23.18 | 31.82 | 14.90 |
| | | Green | 18.14 | 24.41 | 13.51 |
| | | Red | 14.75 | 19.61 | 12.39 |
| | | IR | 9.49 | 12.17 | 11.40 |
| | MA300C | UV | 40.57 | 52.19 | 16.18 |
| | | Blue | 24.46 | 31.57 | 14.26 |
| | | Green | 22.81 | 29.25 | 13.37 |
| | | Red | 22.16 | 29.63 | 12.27 |
| | | IR | 17.68 | 21.21 | 11.32 |

Table S4: Results of the linear relationship of normalized responses from MA300s and AE33

| <i>Parameter</i> | <i>Device</i> | <i>Reg</i> | | <i>WF</i> | |
|------------------------------|---------------|----------------------|----------------------|----------------------|----------------------|
| | | <i>Slope ± error</i> | <i>R²</i> | <i>Slope ± error</i> | <i>R²</i> |
| <i>eBC</i> | MA300A | 1.03 ± 0.01 | 0.86 | 1.06 ± 0.02 | 0.95 |
| | MA300B | 1.19 ± 0.01 | 0.86 | 1.27 ± 0.02 | 0.94 |
| | MA300C | 0.85 ± 0.01 | 0.87 | 0.95 ± 0.02 | 0.94 |
| <i>b_{abs,UV}</i> | MA300A | 0.86 ± 0.01 | 0.88 | 0.86 ± 0.02 | 0.92 |
| | MA300B | 0.80 ± 0.01 | 0.87 | 0.79 ± 0.02 | 0.92 |
| | MA300C | 0.91 ± 0.01 | 0.88 | 0.71 ± 0.01 | 0.91 |
| <i>b_{abs,Blue}</i> | MA300A | 0.85 ± 0.01 | 0.88 | 1.02 ± 0.02 | 0.94 |
| | MA300B | 0.91 ± 0.01 | 0.87 | 0.97 ± 0.02 | 0.93 |
| | MA300C | 0.83 ± 0.01 | 0.88 | 0.91 ± 0.02 | 0.93 |
| <i>b_{abs,Green}</i> | MA300A | 0.87 ± 0.01 | 0.88 | 1.04 ± 0.02 | 0.94 |
| | MA300B | 0.92 ± 0.01 | 0.87 | 1.04 ± 0.02 | 0.93 |
| | MA300C | 0.89 ± 0.01 | 0.88 | 0.98 ± 0.02 | 0.93 |
| <i>b_{abs,Red}</i> | MA300A | 0.89 ± 0.01 | 0.88 | 1.02 ± 0.02 | 0.94 |
| | MA300B | 0.94 ± 0.01 | 0.87 | 1.11 ± 0.02 | 0.93 |
| | MA300C | 0.91 ± 0.01 | 0.87 | 1.03 ± 0.02 | 0.93 |
| <i>b_{abs,IR}</i> | MA300A | 0.91 ± 0.01 | 0.87 | 1.01 ± 0.02 | 0.94 |
| | MA300B | 0.99 ± 0.01 | 0.87 | 1.16 ± 0.02 | 0.93 |
| | MA300C | 0.88 ± 0.01 | 0.87 | 0.97 ± 0.02 | 0.94 |

Table S5: Mean ± standard deviation of eBC (µg/m³) components estimated from diurnal distribution from AE33, MA300 and MA300 with modified Drinovec corrected data

| Period | Wavelength | AE33 | | MA300 | | MA300+Drinovec | |
|---------------|-------------------|-------------------------|-------------------------|-------------------------|-------------------------|-------------------------|-------------------------|
| | | eBC_{bb} | eBC_{ff} | eBC_{bb} | eBC_{ff} | eBC_{bb} | eBC_{ff} |
| Reg | UV-IR | 0.17±0.04 | 1.14±0.36 | 0.12±0.02 | 1.09±0.29 | 0.13±0.03 | 1.24±0.32 |
| | Blue-IR | 0.24±0.05 | 0.91±0.31 | 0.17±0.03 | 0.95±0.26 | 0.18±0.04 | 1.08±0.28 |
| WF | UV-IR | 1.90±0.32 | 1.99±0.79 | 1.07±0.25 | 2.66±0.64 | 0.87±0.27 | 3.61±0.80 |
| | Blue-IR | 1.46±0.23 | 1.73±0.64 | 0.98±0.21 | 2.24±0.55 | 1.17±0.25 | 2.6±0.67 |

Table S6: Filter Loadings experienced by aethalometers during the measurement periods.

| Device | Filter Loading (µg/cm²) | | Filter Loading per unit volume of air sampled (µg/cm²/mL) | |
|---------------|---|-----------|---|-----------|
| | Reg | WF | Reg | WF |
| AE33 | 5.8 | 19.0 | 0.002 | 0.006 |
| MA300A | 1.63 | 5.49 | 0.016 | 0.055 |
| MA300B | 1.46 | 4.85 | 0.015 | 0.049 |
| MA300C | 1.96 | 5.79 | 0.020 | 0.058 |

Figure S2: Wildfire smoke impact on eBC concentration

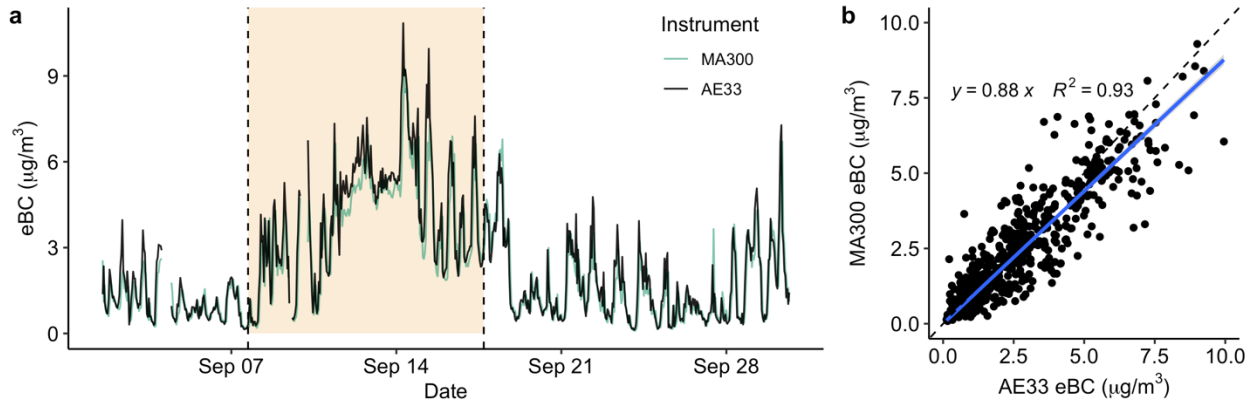


Figure S2: Hourly eBC concentration measured by AE33 and mean of three MA300 units for September 2020 at Clark Drive. (a) Time series of the measurements with the yellow shaded region representing the wildfire smoke affected days (Sep 8 – Sep 18). (b) Scatter plot of the same data with liner fit (blue line). Dashed line represents the 1:1 line

Figure S3: Wavelength specific b_{abs} from AE33

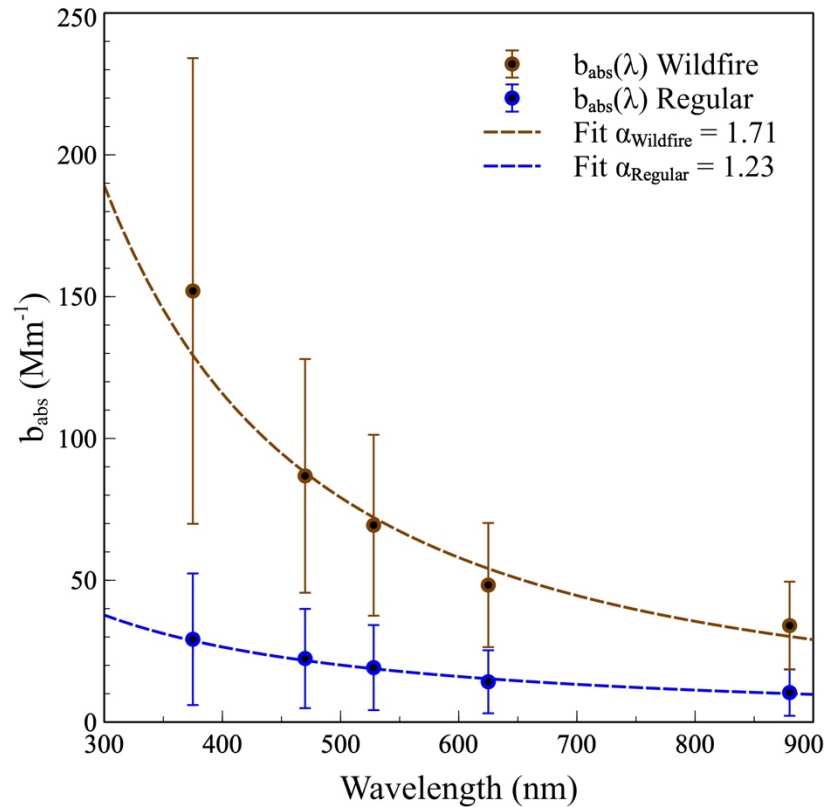


Figure S3: Mean b_{abs} values measured during the Regular and Wildfire days by AE33 across five wavelengths. Error bar represents the standard deviation, and the dashed line represents the power law fit. α (exponent of the power law fit) has been mentioned for the two periods.

Figure S4: Wavelength specific b_{abs} from MA300

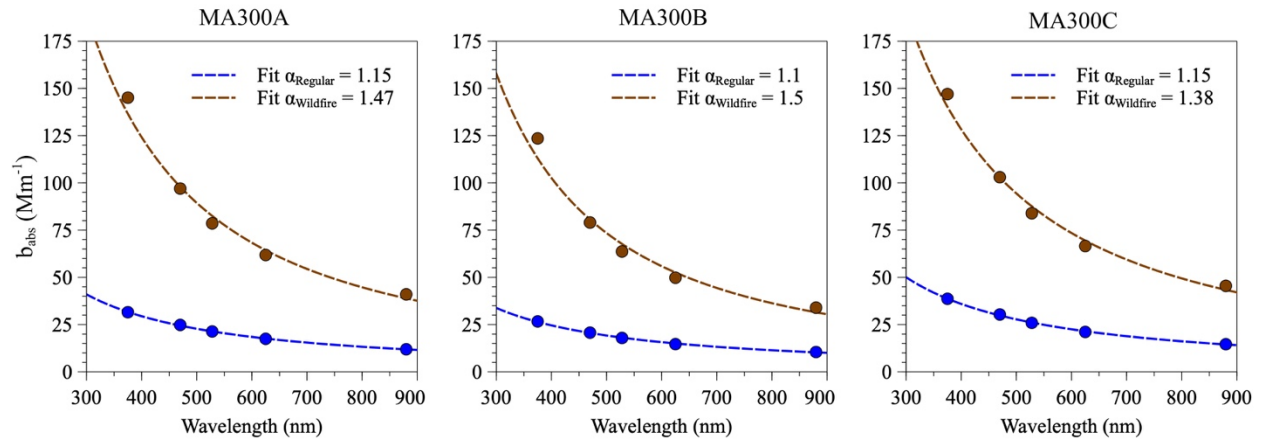


Figure S4: Mean b_{abs} values measured during Regular and Wildfire days by MA300A, MA300B and MA300C across five wavelengths. The dashed line represents the power law fit. α (exponent of the power law fit) has been mentioned for the two periods.

Figure S5: Comparison of source apportionment results with wavelength pairs used

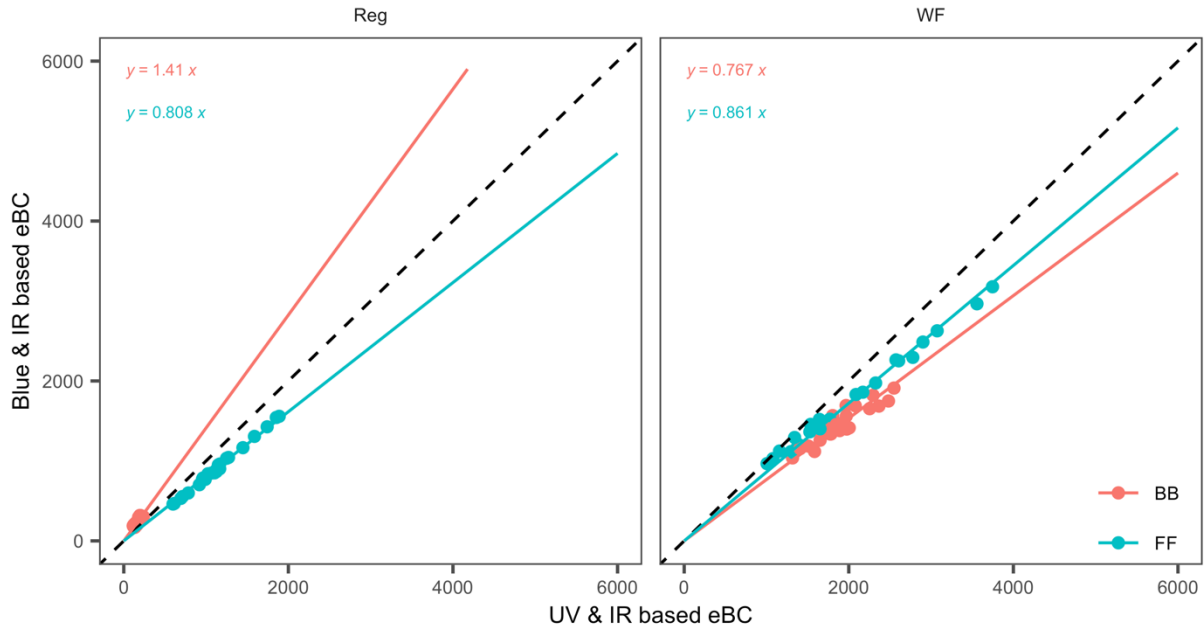


Figure S5: Comparison of AE33 reported diurnal hourly eBC (ng/m³) contribution from eBC_{bb} and eBC_{ff} from UV-IR based and Blue-IR based source apportionment techniques

Figure S6: MA300 Source Apportionment Result from Modified Drinovec Correction

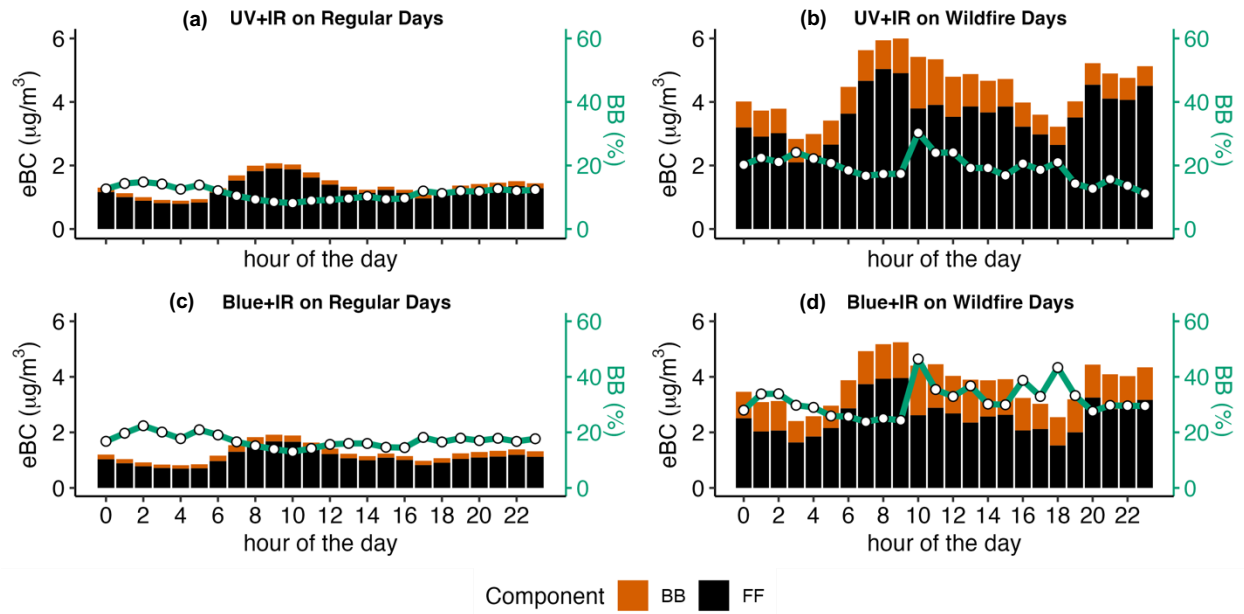


Figure S6: Diurnal variation of Modified Drinovec corrected (on MA300s) eBC contribution from BB and FF sources during regular (Reg) days and wildfire smoke affected (Wildfire) days. Panels A-B are for the UV-IR pairs, and Panels C-D are for the Blue-IR pairs. Wildfire smoke-affected days are in Panels B and D, and Regular days are in panels A and C. The green line (right axis) represents the percentage of eBC mass from biomass burning during the measurement period.

Figure S7: Variability of eBC measurement by MA300

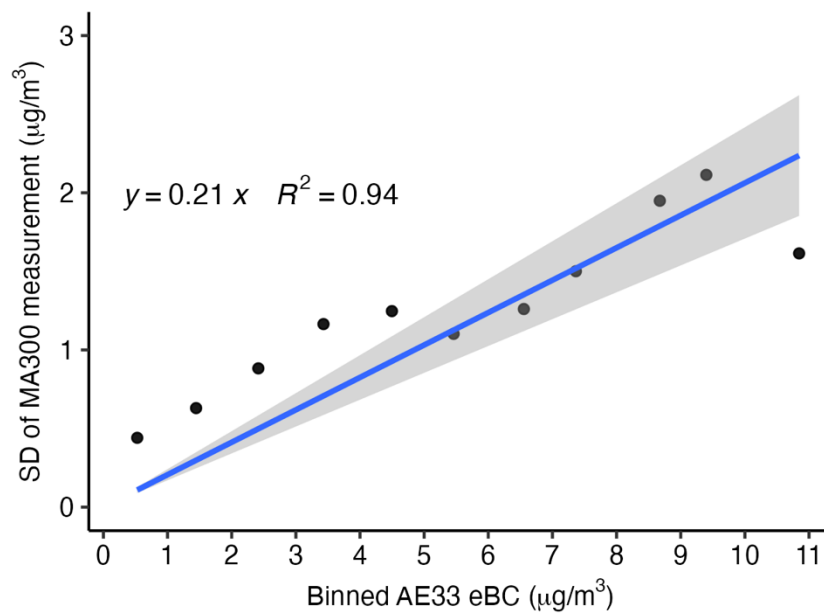


Figure S7: Multi unit pooled standard deviation from MA300 measurements for each one $\mu\text{g m}^{-3}$ of eBC concentration measured by AE33. The fit line (in blue) represents the linear response of MA300's variability across the concentration range. The shaded region represents the 95% CI of the fit

Figure S8: AE33's spectral change in normalized b_{abs}

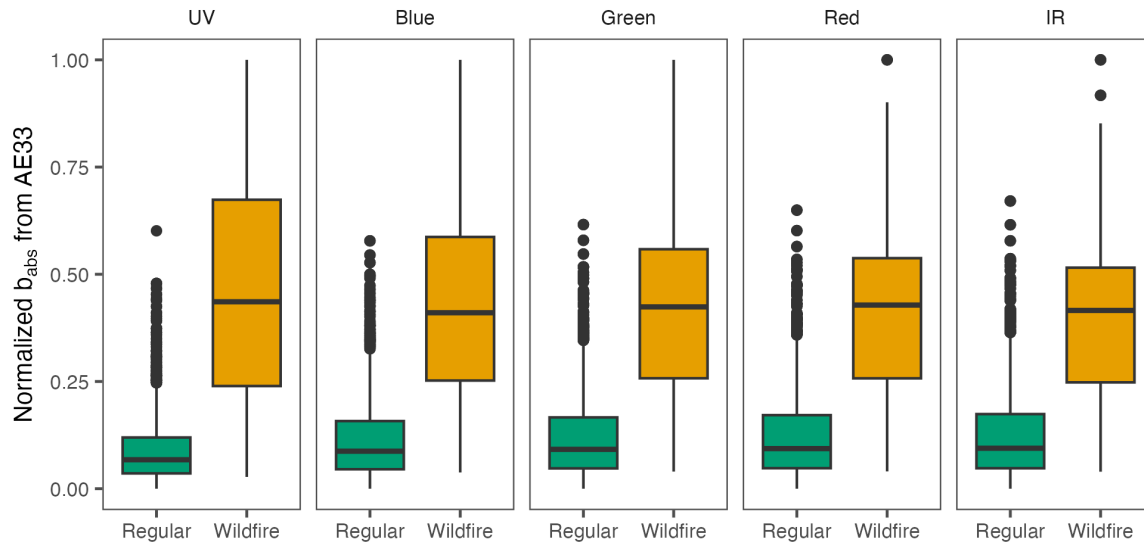


Figure S8: Box plot of normalized b_{abs} from AE33 over the five channels categorized by the measurement period. Increased median values during the Wildfire period can be identified from the horizontal lines of each boxplot.

Figure S9: Density plot of Ångström exponent (α)

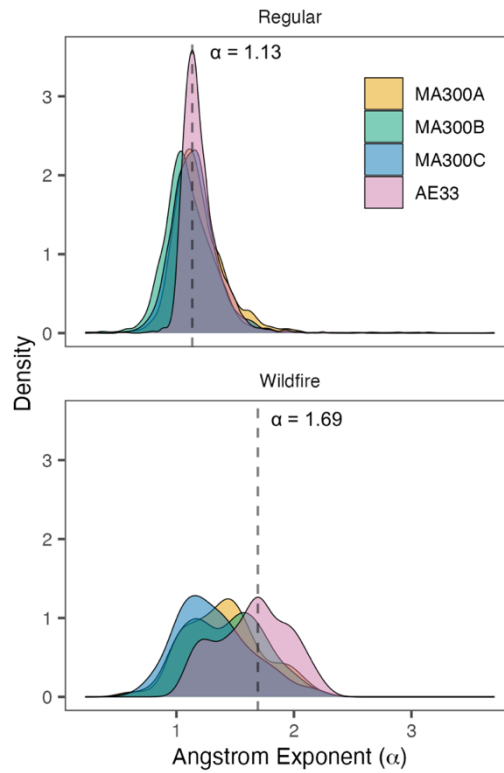


Figure S9: Distribution of Ångström Exponent (α) from the four aethalometers during regular (top) and wildfire (bottom) period. The α values have been calculated from hourly estimates of UV and IR b_{abs} values. Vertical dashed line represents the peak of the distributions from AE33 measurements for individual period.

Figure S10: Sensitivity analysis of Aethalometer Source Apportionment Model on UV-IR pair

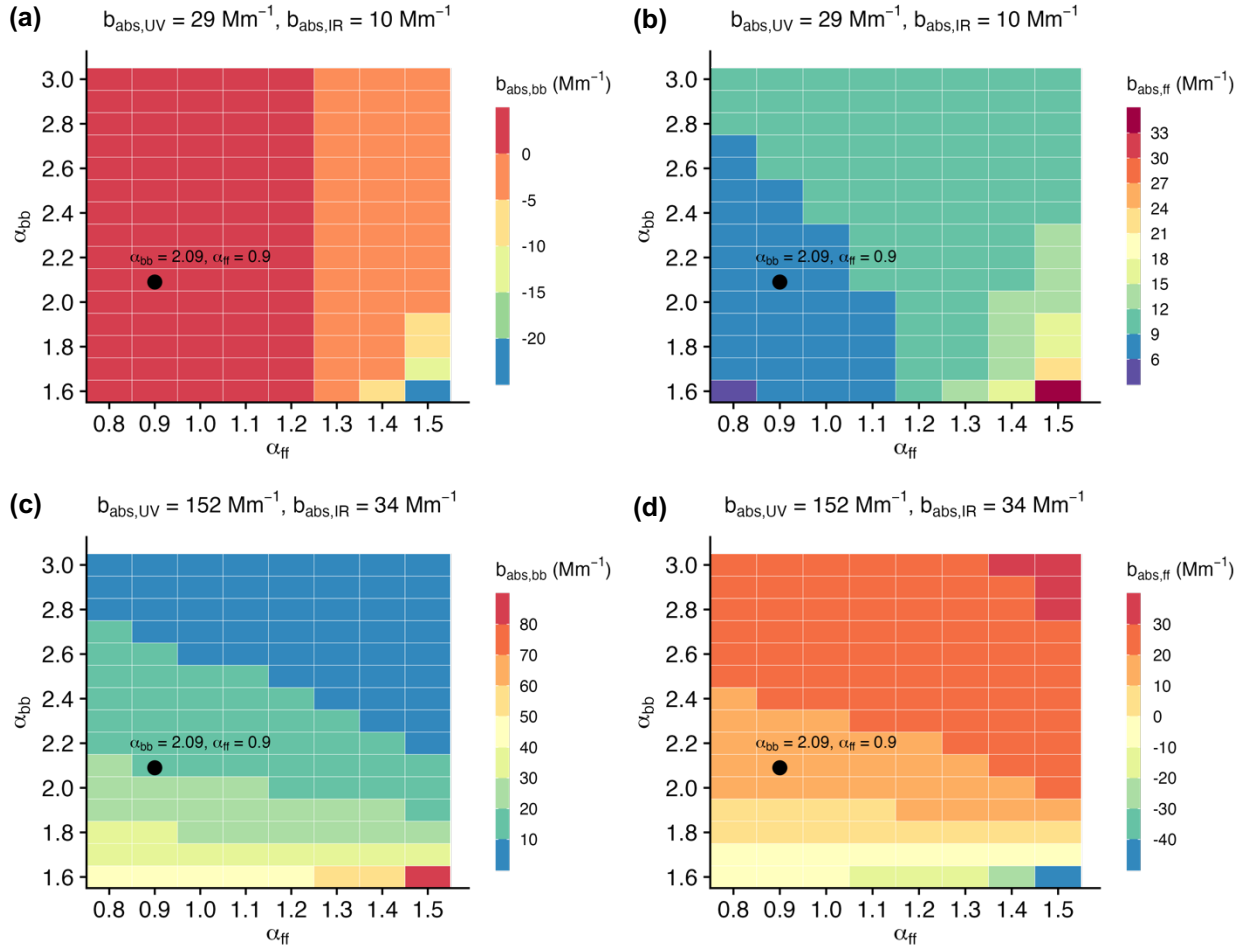


Figure S10: Sensitivity analysis on UV-IR wavelength pair done with α_{ff} range of 0.8-1.5 and α_{bb} range of 1.6-3.0. Panel A and B represents the $b_{abs,bb}$ and $b_{abs,ff}$ components derived from the AE33's average b_{abs} values for the regular period. Panel C and D represents the same but for the AE33's average b_{abs} values for the wildfire period. Black dot represent the α pair considered in the source apportionment method.

For Sensitivity analysis we used AE33's mean b_{abs} concentrations for UV, Blue and IR channels from the Regular and Wildfire period with α_{bb} range 1.6 -- 3.0 and α_{ff} range 0.8 -- 1.5. Mean values have been taken from Table 1. Since, aethalometer model responses can vary based on the input b_{abs} data, we chose to test the results for these cases:

1. Regular Day
 - a. $b_{abs,UV} = 29 \text{ Mm}^{-1}$, $b_{abs,IR} = 10 \text{ Mm}^{-1}$
 - b. $b_{abs,Blue} = 23 \text{ Mm}^{-1}$, $b_{abs,IR} = 10 \text{ Mm}^{-1}$
2. Wildfire Day
 - a. $b_{abs,UV} = 152 \text{ Mm}^{-1}$, $b_{abs,IR} = 34 \text{ Mm}^{-1}$
 - b. $b_{abs,Blue} = 87 \text{ Mm}^{-1}$, $b_{abs,IR} = 34 \text{ Mm}^{-1}$

We identify that minimum detection limit of MA300s can impact the measurement and so as the source apportionment results. Therefore use estimate MDL (Hyslop et al., 2022) from the particle free measurement data as utilized for characterizing noise. The noise as defined by (Cuesta-Mosquera et al., 2021) and MDL could be scientifically similar, however, we wanted to check if there is any influence of MDL on MA300's measurement. MDL has been estimated as $0.21 \mu\text{g m}^{-3}$

Figure S11: Sensitivity analysis of Aethalometer Source Apportionment Model on Blue-IR pair

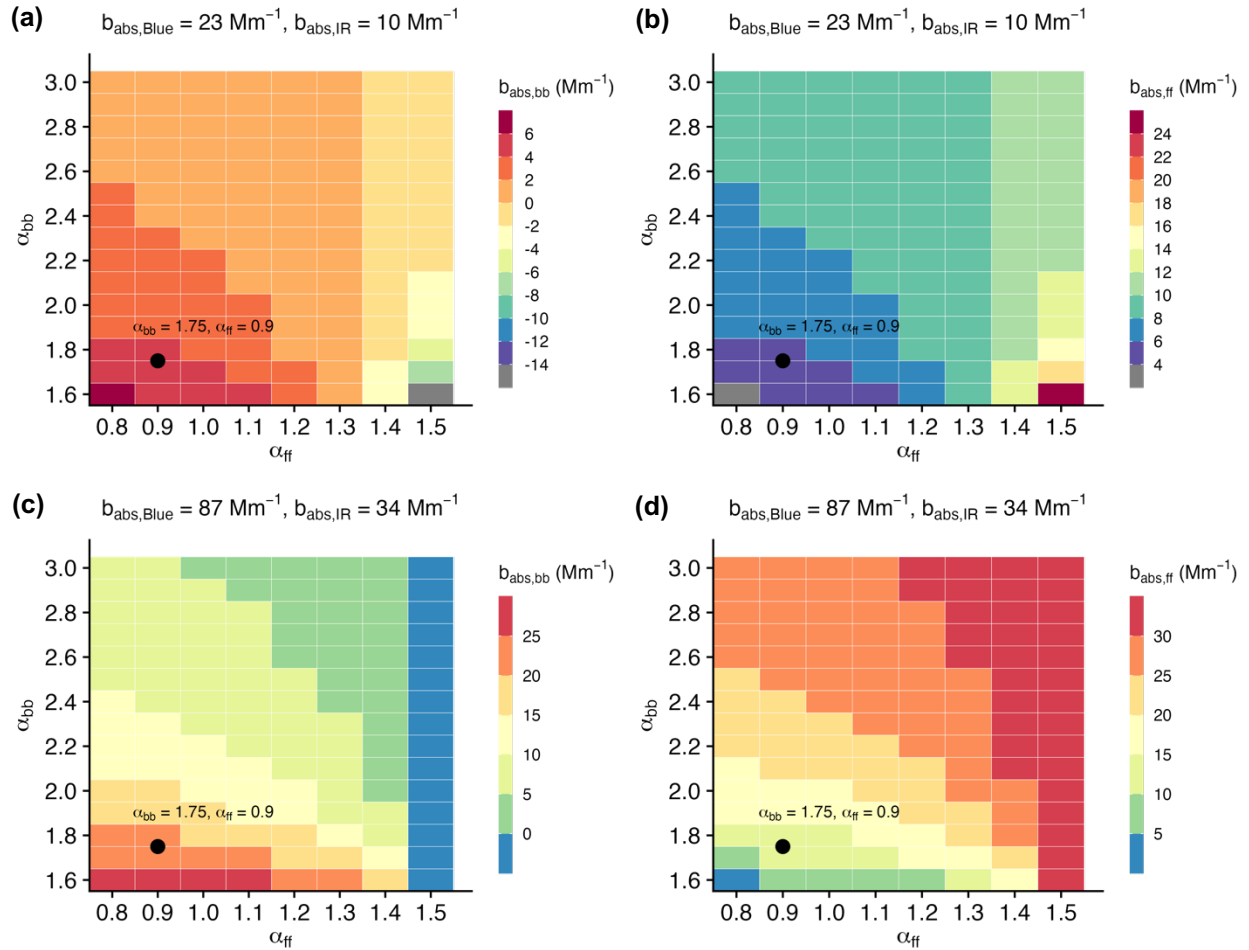


Figure S11: Sensitivity analysis on Blue-IR wavelength pair done with α_{ff} range of 0.8-1.5 and α_{bb} range of 1.6-3.0. Panel A and B represents the $b_{\text{abs,bb}}$ and $b_{\text{abs,ff}}$ components derived from the AE33's average b_{abs} values for the regular period. Panel C and D represents the same but for the AE33's average b_{abs} values for the wildfire period. Black dot represent the α pair considered in the source apportionment method

Figure S12: Source Apportionment results from AE33 for either side of wildfire period

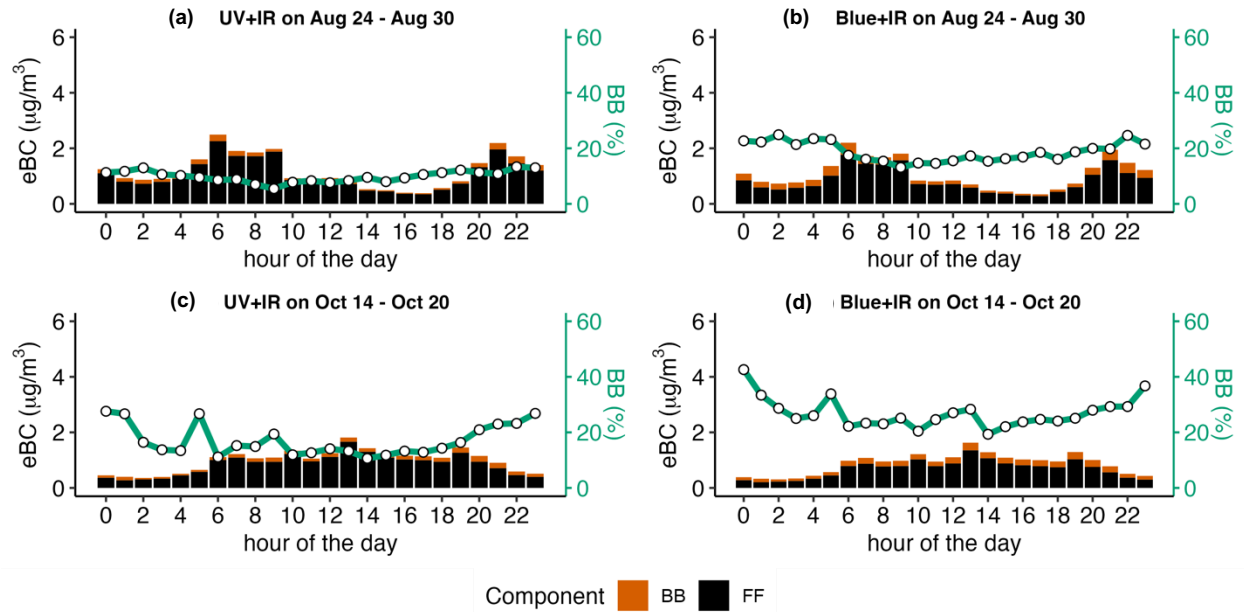


Figure S12: Diurnal variation of AE33 reported eBC contribution from biomass burning (BB) and fossil fuel (FF) sources for two specific periods. Panel A (UV-IR pair) and B (Blue-IR pair) represents pre-wildfire period: August 24 to August 30. Panel C (UV-IR pair) and D (Blue-IR pair) represents post-wildfire period: October 14 to October 20. The green line (right axis) represents the percentage of eBC mass from biomass burning during the measurement periods.

Figure S13: Percentage difference source apportionment results from MA300's modified

Drinovec corrected data

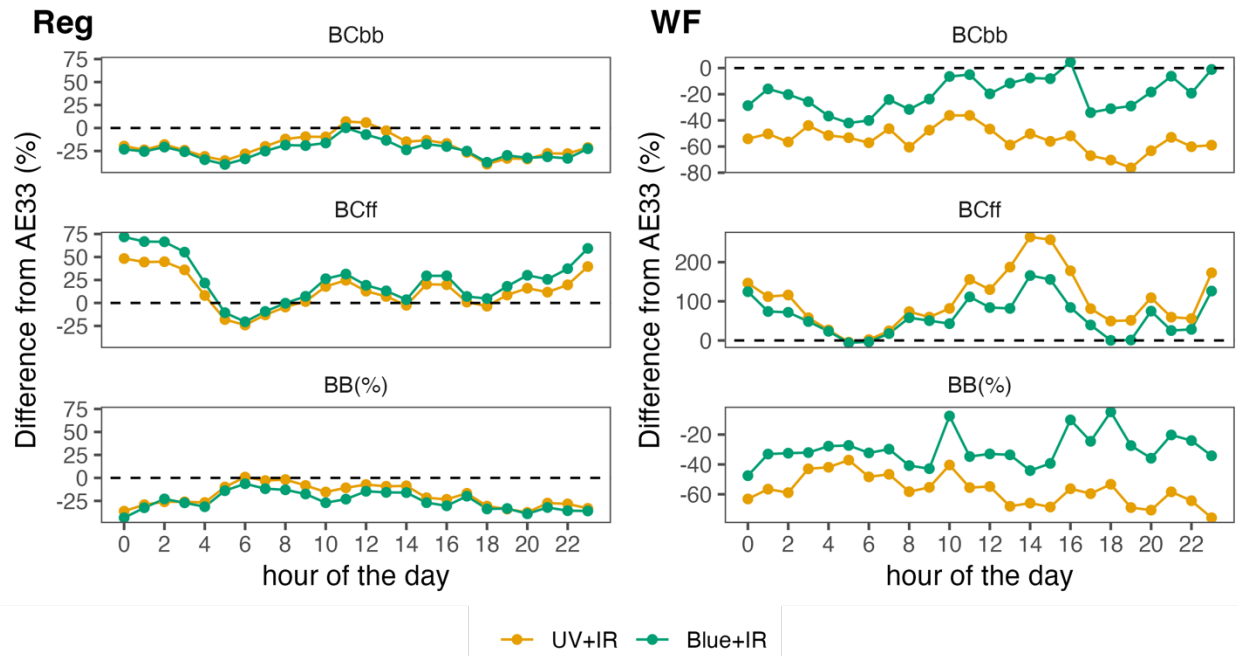


Figure S13 Percentage difference of hourly SA results in between MA300 and AE33. Average Drinovec- corrected MA300 are data treated separately for the two periods (Reg and WF). SA results from UV-IR and Blue-IR wavelength pair have been evaluated separately

Section F: A case study on MA300's eBC measurement during high PM event

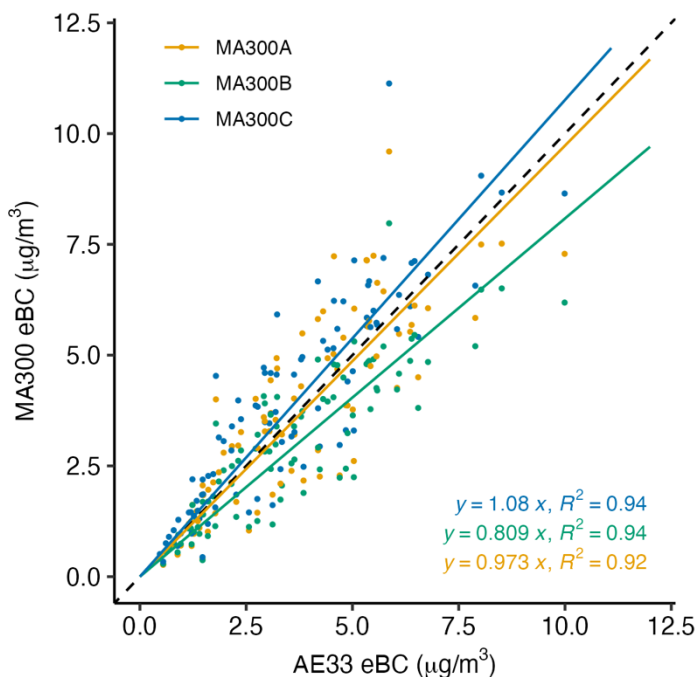


Figure S14: Scatter plot of eBC mass concentration for individual MA300 units A, B and C vs AE33 during the high PM event. The dashed line represents the 1:1 line, and solid colors are the regression fit lines for the individual MA300 units

During the Regular days, a specific high PM event was identified in this study. These days were October 31st to November 2nd and were impacted by the local fireworks from Halloween celebrations. We removed these data points from the main analysis to improve the data consistency in the Regular period. We find good linear association ($R^2 > 0.9$) across the MA300 units, when compared against the reference device AE33. Slope from the linear fit of these three MA300 devices were slightly higher than reported values in the main text (Figure 1(a)), however the patterns remain the same. The mean eBC concentration were found as 3.6, 3.0 and 3.9 $\mu\text{g}/\text{m}^3$ from MA300A, MA300B and MA300C respectively. Mean eBC concentration reported by the reference AE33 was 3.55 $\mu\text{g}/\text{m}^3$. These mean eBC concentrations were much higher than the rest of the days during the Regular period and highlights the importance of marking associated events while collecting data which could potentially impose bias in the analysis.

Reference:

Alas, H. D. C., Müller, T., Weinhold, K., Pfeifer, S., Glojek, K., Gregorič, A., Močnik, G., Drinovec, L., Costabile, F., Ristorini, M., and Wiedensohler, A.: Performance of microAethalometers: Real-world Field Intercomparisons from Multiple Mobile Measurement Campaigns in Different Atmospheric Environments, *Aerosol Air Qual. Res.*, 20, 2640–2653, <https://doi.org/10.4209/aaqr.2020.03.0113>, 2020.

Cuesta-Mosquera, A., Močnik, G., Drinovec, L., Müller, T., Pfeifer, S., Minguillón, M. C., Briel, B., Buckley, P., Dudoitis, V., Fernández-García, J., Fernández-Amado, M., Ferreira De Brito, J., Riffault, V., Flentje, H., Heffernan, E., Kalivitis, N., Kalogridis, A.-C., Keernik, H., Marmureanu, L., Luoma, K., Marinoni, A., Pikridas, M., Schauer, G., Serfozo, N., Servomaa, H., Titos, G., Yus-Díez, J., Zioła, N., and Wiedensohler, A.: Intercomparison and characterization of 23 Aethalometers under laboratory and ambient air conditions: procedures and unit-to-unit variabilities, *Atmospheric Measurement Techniques*, 14, 3195–3216, <https://doi.org/10.5194/amt-14-3195-2021>, 2021.

Drinovec, L., Močnik, G., Zotter, P., Prévôt, A. S. H., Ruckstuhl, C., Coz, E., Rupakheti, M., Sciare, J., Müller, T., Wiedensohler, A., and Hansen, A. D. A.: The “dual-spot” Aethalometer: an improved measurement of aerosol black carbon with real-time loading compensation, *Atmospheric Measurement Techniques*, 8, 1965–1979, <https://doi.org/10.5194/amt-8-1965-2015>, 2015.

Dumka, U. C., Kaskaoutis, D. G., Tiwari, S., Safai, P. D., Attri, S. D., Soni, V. K., Singh, N., and Mihalopoulos, N.: Assessment of biomass burning and fossil fuel contribution to black carbon concentrations in Delhi during winter, *Atmospheric Environment*, 194, 93–109, <https://doi.org/10.1016/j.atmosenv.2018.09.033>, 2018.

Géron, A.: *Hands-On Machine Learning with Scikit-Learn, Keras, and TensorFlow*, O'Reilly Media, Inc., 879 pp., 2022.

Healy, R. M., Wang, J. M., Sofowote, U., Su, Y., Deboisz, J., Noble, M., Munoz, A., Jeong, C.-H., Hilker, N., Evans, G. J., and Doerksen, G.: Black carbon in the Lower Fraser Valley, British Columbia: Impact of 2017 wildfires on local air quality and aerosol optical properties, *Atmospheric Environment*, 217, 116976, <https://doi.org/10.1016/j.atmosenv.2019.116976>, 2019.

Hyslop, N. P., Liu, Y., Yarkin, S., and Trzepla, K.: Application of the U.S. EPA procedure for determining method detection limits to EDXRF measurement of filter-based aerosol samples, *Journal of the Air & Waste Management Association*, 72, 905–913, <https://doi.org/10.1080/10962247.2022.2064005>, 2022.

Krstic, G., Krstic, N., and Zambrano-Bigiarini, M.: The br2 – weighting Method for Estimating the Effects of Air Pollution on Population Health, *Journal of Modern Applied Statistical Methods*, 15, <https://doi.org/10.22237/jmasm/1478004000>, 2016.

Malings, C., Tanzer, R., Hauryliuk, A., Kumar, S. P. N., Zimmerman, N., Kara, L. B., Presto, A. A., and R. Subramanian: Development of a general calibration model and long-term performance evaluation of low-cost sensors for air pollutant gas monitoring, *Atmos. Meas. Tech.*, 12, 903–920, <https://doi.org/10.5194/amt-12-903-2019>, 2019.

Rajesh, T. A. and Ramachandran, S.: Characteristics and source apportionment of black carbon aerosols over an urban site, *Environ Sci Pollut Res*, 24, 8411–8424, <https://doi.org/10.1007/s11356-017-8453-3>, 2017.

Rajesh, T. A. and Ramachandran, S.: Black carbon aerosol mass concentration, absorption and single scattering albedo from single and dual spot aethalometers: Radiative implications, *Journal of Aerosol Science*, 119, 77–90, <https://doi.org/10.1016/j.jaerosci.2018.02.001>, 2018.

Sandradewi, J., Prévôt, A. S. H., Szidat, S., Perron, N., Alfarra, M. R., Lanz, V. A., Weingartner, E., and Baltensperger, U. R. S.: Using aerosol light absorption measurements for the quantitative determination of wood burning and traffic emission contribution to particulate matter, *Environmental Science and Technology*, 42, 3316–3323, <https://doi.org/10.1021/es702253m>, 2008.

Virkkula, A., Mäkelä, T., Hillamo, R., Yli-Tuomi, T., Hirsikko, A., Hämeri, K., and Koponen, I. K.: A Simple Procedure for Correcting Loading Effects of Aethalometer Data, *Journal of the Air & Waste Management Association*, 57, 1214–1222, <https://doi.org/10.3155/1047-3289.57.10.1214>, 2007.

Yao, J., Brauer, M., and Henderson, S. B.: Evaluation of a Wildfire Smoke Forecasting System as a Tool for Public Health Protection, *Environmental Health Perspectives*, 121, 1142–1147, <https://doi.org/10.1289/ehp.1306768>, 2013.

Zambrano-Bigiarini, M.: Package ‘hydroGOF,’ Goodness-of-fit Functions for Comparison of Simulated and Observed, 2020.

Zimmerman, N.: Tutorial: Guidelines for implementing low-cost sensor networks for aerosol monitoring, *Journal of Aerosol Science*, 159, 105872, <https://doi.org/10.1016/j.jaerosci.2021.105872>, 2022.

Zotter, P., Herich, H., Gysel, M., El-Haddad, I., Zhang, Y., Močnik, G., Hüglin, C., Baltensperger, U., Szidat, S., and Prévôt, A. S. H.: Evaluation of the absorption Ångström exponents for traffic and wood burning in the Aethalometer-based source apportionment using radiocarbon measurements of ambient aerosol, *Atmospheric Chemistry and Physics*, 17, 4229–4249, <https://doi.org/10.5194/acp-17-4229-2017>, 2017.